ISSN 1069-3513, Izvestiya, Physics of the Solid Earth, 2008, Vol. 44, No. 7, pp. 555–569. © Pleiades Publishing, Ltd., 2008.
Original Russian Text © A.F. Grachev, O.A. Korchagin, V.A. Tselmovich, H.A. Kollmann, 2008, published in Fizika Zemli, 2008, No. 7, pp. 42–57.

# Cosmic Dust and Micrometeorites in the Transitional Clay Layer at the Cretaceous–Paleogene Boundary in the Gams Section (Eastern Alps): Morphology and Chemical Composition

**A. F. Grachev[a], O. A. Korchagin[b], V. A. Tselmovich[a], and H. A. Kollmann[c]**

[a] *Schmidt Institute of Physics of the Earth, Russian Academy of Sciences (RAS), Bol'shaya Gruzinskaya ul. 10, Moscow, 123995 Russia*

[b] *Geological Institute, RAS, Pyzhevskii per. 7, Moscow, 119017 Russia*

[c] *Museum of Natural History, Vienna, Austria*

Received December 3, 2007

**Abstract**—Results of investigation of the cosmic substance in the transitional clay layer at the Cretaceous–Paleogene boundary in the Gams section, Eastern Alps, are presented. A great diversity of iron microspherules and particles of different morphologies, pure nickel spherules, awaruite ($Fe_3Ni$) particles, and diamond crystals are discovered. Iron microspherules are also met in the overlying Paleocene deposits, but their diversity there is not great. The discovered metallic microspherules and particles are described, their chemical compositions are presented, and their origin is discussed.

PACS numbers: 91.67.Gy

**DOI:** 10.1134/S1069351308070069

## INTRODUCTION

Investigations of cosmic dust in sedimentary rocks were inspired by the results of the H.M.S. *Challenger* cruise, during which traces of cosmic matter were discovered for the first time in red deep-sea clays [Murray and Renard, 1891]. Samples of ferromanganese nodules and magnetic microspherules up to 100 μm in diameter, which were later called cosmic spherules, were uplifted from a depth of 4300 m during the dredging at two stations in the southern Pacific. However, the iron microspherules gathered by *Challenger* were studied only in recent years. It was found out that internal parts of the spherules consist of metallic iron (90%) and nickel (10%), whereas their surfaces are covered by thin crusts of iron oxide [Jedwab, http://www.ub.ac.be/sciences/cosmicdust.pdf].

In fact, the study of cosmic matter was initiated by the discovery of cosmic spherules in deep-sea clays. However, this problem excited great interest of researchers only after first launches of cosmic vehicles that could sample lunar ground and dust particles in various regions of the solar system. Studies of the Tunguska catastrophe traces and meteoritic dust sampled in the place of the fall of the Sikhote-Alin' meteorite also played an important role [Florensky, 1963; Florensky et al., 1968; Ivanov and Florensky, 1970; Krinov, 1971].

Interest in metallic microspherules displayed by a wide range of researchers has led to the discovery of the microspherules in sedimentary rocks of different ages and origins. For example, metallic microspherules have been found in ices of Antarctic and Greenland [Maurette et al., 1986; Yada et al., 2004], deep-sea oceanic sediments and manganese nodules [Hunter and Parkin, 1960; Finkelman, 1970; Parkin et al., 1980; Brownlee et al., 1984; Brownlee, 1985], and sands of deserts and beaches [Marvin and Einaudi, 1967]. Thousands of Fe–Ni alloy spherules from Pleistocene deposits of Alberta (Canada) [Bi et al., 1993] and magnetite microspherules from Holocene fluvioglacial deposits of the Carpathians [Szoor et al., 2001] have been studied. Metallic particles and microspherules are often met in and near meteoritic craters [El Coresy, 1966; Florensky et al., 1968; Sobotovich et al., 1978; Raukas, 2000; Stankowski et al., 2006].

Metallic microspherules of extraterrestrial origin are known in sedimentary rocks of various ages: Lower and Upper Cambrian [Raukas, 2000; Korchagin et al., 2007], Ordovician [Schmitz et al., 1996], and Permian, Triassic, and Jurassic [Miono et al., 1993; Chapman and Lauretta, 2004]. Higher concentrations of metallic microspherules of extraterrestrial origin are noted near the Permian–Triassic and Triassic–Jurassic boundaries [Miono et al., 1993] and near the Cretaceous–Paleogene boundary [Smit and Romein, 1985; Ebihara and Miura, 1996].

Data on microspherules and particles from ancient deposits provide insights into volumes of cosmic matter coming to the Earth, the pattern (uniform or nonuniform) of this influx, variations in the composition of cosmic particles arriving at the Earth, primary sources of this substance, and the influence of these processes

on the evolution of life on the Earth. Many of these problems are still far from being solved; however, the accumulation of data and their comprehensive study are undoubtedly favorable for the solution of these problems.

Thus, it is known that the total mass of dust circulating inside the Earth's orbit is about $10^{15}$ t and, according to various estimates, 4000 to 10000 t of the cosmic substance falls annually onto the Earth's surface [Sobotovich, 1976; Karner et al., 2003; Yada et al., 2004]; particles 50–400 μm in size account for 95% of this substance [Kurat et al., 1994]. As for time variations in the rate of the influx of cosmic substance to the Earth, this question has remained controversial as yet, notwithstanding a great number of investigations carried out during the past decade.

There is the opinion that the influx rate of cosmic dust with the planetary ratio of helium isotopes $^3He/^4He$ ($10^{-4}$) varies weakly with time [Karner et al., 2003; Winckler and Fisher, 2006]; however, directly opposite data are also available [Farley, 1995; Schmitz et al., 1996]. Note that all known estimates are obtained for different time intervals (from hundreds of thousands to tens of millions of years), and the rate is known to depend strongly on the interval of averaging. This is indirectly indicated also by data on variations in the ratio of helium isotopes $^3He/^4He$ at the Cretaceous–Paleogene boundary in the Gams section [Grachev et al., 2007].

The study of present-day cosmic dust is based on investigations of deep-sea deposits and the glacial cover in Greenland and Antarctic and samples taken from the stratosphere [Brownlee, 1985]. According to present based on particle sizes, cosmic dust is subdivided into interplanetary cosmic dust proper (IDPs) with particle sizes smaller than 30 μm and micrometeorites with particle sizes larger than 50 μm [Genge et al., 1997]. Krinov [1971] proposed that the finest molten surface fragments of a meteoric body be called micrometeorites. Such a classification is naturally rather arbitrary and, as demonstrated below, in the Gams section we found molten fragments of pure iron a few microns in size; we propose them to be called nanometeorites rather than micrometeorites. Moreover, meteoritic dust, meteoritic iron, and impactites are also distinguished at present [Raukas, 2000]. No rigorous criteria for the discrimination between cosmic dust and meteoritic particles have been developed as yet, and even the example of the Gams section we studied shows that metallic particles and microspherules differ in shape and composition more significantly than is provided for by the existing classifications. Thus, the virtually perfect spherical shape, metallic luster, and magnetic properties of particles were regarded as evidence for their cosmic origin. According to Sobotovich [1976, p. 107], "the presence of molten spherules, including magnetic ones, is the only morphological criterion for distinguishing the cosmic origin of material studied." A surface texture of microspherules is also regarded as evidence indicating that they belong to the category of meteoritic dust. However, apart from shapes that are very diverse, the substance composition is of fundamental importance as is shown below [Grachev et al., 2006]. Studies of metallic microspherules (spherules) showed that, along with microspherules of cosmic origin, there is a great amount of spherules of other geneses, such as volcanic activity, vital activity of bacteria, or metamorphism. It is known that Fe microspherules of volcanic origin rarely have a perfect spherical shape and are distinguished by a higher concentration of Ti admixture (more than 10%).

The origin of cosmic dust is still the subject of discussion. According to Sobotovich [1976], cosmic dust can represent remains of the primordial protoplanetary cloud. This suggestion was disputed by Levin and Simonenko [1973], who believed that the primordial finely dispersed substance has not been preserved.

According to an alternative explanation, the formation of cosmic dust is associated with destruction of asteroids and comets. Sobotovich [1976] notes that, if the amount of cosmic dust supplied to the Earth does not change with time (for example, throughout the Phanerozoic), Levin and Simonenko [1973] are right.

Notwithstanding a great volume of research, this fundamental question cannot be answered at present because quantitative estimates are few and their accuracy raises doubts. Data of IDP isotope studies using particles gathered in the stratosphere in the framework of the NASA program suggest the existence of particles of presolar origin [Messenger et al., 2003]. Moreover, it was found that the same dust contains such minerals as corundum, moissanite, and diamond, whose origin can be referred to the time before the solar system formation according to data of the carbon and nitrogen isotopy [Stadermann et al., 2006].

We should note that a similar mineral assemblage (diamond, moissanite, and corundum) was discovered in the boundary layer at the K/T boundary in the Gams section [Grachev et al., 2005, 2006]. The above brief review clearly indicates that the study of cosmic dust in a geological section is very important. This paper presents the first results of the study of the cosmic substance in the transitional clay layer at the Cretaceous–Paleogene boundary in the Gams section, Eastern Alps [Grachev et al., 2005].

## DATA AND GENERAL CHARACTERISTICS OF THE GAMS SECTION

This paper is based on data obtained from several sections of Cretaceous–Paleogene transition layers located near Gams village in Stiria, where the Gams River exposes the K/T boundary in several places. The general geological position of the section in the Gams area (Knappengraben) was previously described by Kollmann [1964] and Lahodynsky [1988], who estab-

lished that this section belongs to the Niernthal formation (chron 29R). The section part below the K/T transition layer is represented by alternating calcareous
2 marl and marly limestone, while the overlying part is dominated by clays with different concentrations of calcium carbonate and isolated beds of a sand–siltstone composition [Grachev et al., 2005].

A monolith was cut from the outcrop of the section Gams 1, where the K/T boundary is very well expressed (Fig. 1). The monolith is 46 cm high, 30 cm wide in its lower part, 22 cm wide in its upper part, and 4 cm thick. For a general study of the section, the monolith was divided (from bottom to top) into 2-cm layers **A**, **B**, **C** … **W**, and each layer was marked at 2-cm intervals (1, 2, 3, etc.). The K/T transition layer *J* was studied in greater detail: six sublayers (units), each about 3 mm thick, were distinguished here (see [Grachev et al., 2005] for more details). As was previously shown, the K/T transition layer of clay contains Fe, Au, and Cu particles. Crystals of Ni-spinel were also found at the base of the layer and in its upper part [Grachev et al., 2007].

The lower four sublayers belong to the *Hedbergella holmdelensis* zone (including the "barren interval"), the upper two sublayers belong to the *Globoconusa daubjergensis* zone (small morphotype), and overlying siltstones belong to the *Subbotina fringa* (lower part) and *Parasubbotina pseudobulloides* (upper part) zones. It was also shown that the transitional clay layer is enriched in Ir, As, Pb, Zn, and Cr [Grachev et al., 2005]. However, we should emphasize that the highest Ir concentrations are confined to the lower and middle parts of the transitional layer, the concentration of this element in its upper part being small.

Results of investigations of the section Gams 1 are in many aspects similar to those obtained for the Gams 2 section (Fig. 2). Here, we present data obtained for both sections.

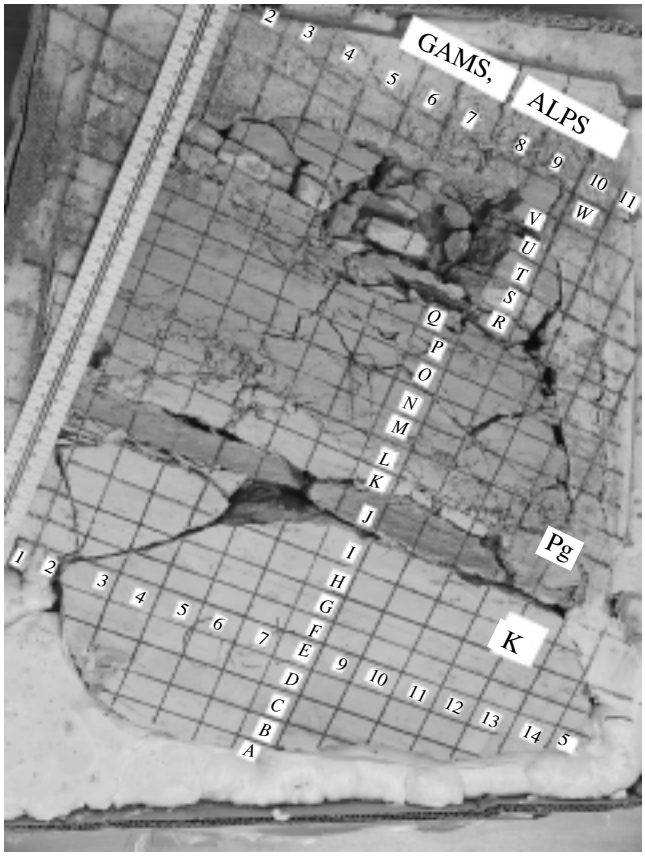


**Fig. 1.** General view of the monolith from the Gams section prepared for sampling. The Cretaceous–Paleogene transition layer is denoted as **J**.

## PREPARATION OF SAMPLES FOR ANALYSIS AND METHODS OF STUDY

The complex of studies included the following procedures: examination of thin sections and monomineral fractions; "wet" chemistry; X-ray fluorescence, neutron activation, and X-ray structural analyses; helium, carbon, and oxygen isotope analysis; microprobe determination of mineral compositions; and magnetomineralogical analysis.

To extract the heavy fraction of minerals, a sample 10–15 g in weight was crushed in a porcelain mortar and screened through a 0.25-mm sieve. The heavy fraction of minerals was separated from the carbonate-clay mass with the use of a heavy liquid (the bromoform $CHBr_3$ of a density of 2.89 g/cm$^3$). The heavy and light fractions were washed by alcohol and separated from the magnetic fraction by a simple magnet. The heavy fraction of minerals was separated with an electromagnetic separator into nonelectromagnetic, weakly electromagnetic, and electromagnetic fractions, which were glued under binoculars to glass slides with a depression.

Compositions and microstructures of magnetic minerals of rocks were determined with a Camebax electron microprobe and, selectively, with a Tescan Vega scanning electron microscope (SEM). Samples were usually mounted in a washer 26 mm in diameter with the use of Wood alloy and carefully ground and polished by diamond pastes, after which they were sprayed with a carbon film. The samples were analyzed with an accelerating voltage of 20 kV and a beam current of 10 nA. Elements determined by the characteristic X-radiation ranged from sodium to uranium. The effective diameter of the probe was about 1–2 μm, which was regularly checked with minor phases. Extracted metallic microspherules and particles were cleaned with ultrasound and etched with acids (HCl) in order to remove an oxide film from the surface. Quantitative microanalysis of ore phases was performed, and the $TiO_2$, FeO, MgO, MnO, $Cr_2O_3$, and $Al_2O_3$ concentrations were measured. This was preceded by qualitative

**Fig. 2.** Cretaceous–Paleogene boundary in the outcrop Gams 2.

analysis for revealing the presence of all elements (from sodium to uranium). The Puma software was used for calculations. Inhomogeneities in selected zones of distributions of the elements were examined using both linear and areal scanning. The minerals (or selected zones) were photographed both with a SEM and in characteristic X rays of Ti, Fe, Mg, Mn, Cr, Al, Si, and Ca.

Nickel and iron particles detected with the Camebax microprobe were additionally examined by A.N. Nekrasov with the Tescan Vega microprobe at the RAS Institute of Experimental Mineralogy, Russian Academy of Sciences. The Tescan Vega microprobe equipped with an energy-dispersion spectrometer measured the carbon content, which allowed us to confirm independently the presence of diamond grains detected by their intense blue luminescence under the Camebax electron probe.

Some grains of the studied minerals were prepared with the use of a specially developed procedure that ensured ultrafine polishing of an object with a removed layer thickness of no more than 5 μm over the entire process. Removal of a layer 5–10 μm thick from iron spherules opened pores 10–20 μm in diameter. The polishing uncovered even hollow metallic cosmic spherules with a wall thickness of 0.5–2 μm. For this purpose, grains extracted with a powerful hand-operated Nb-B-Fe magnet were placed on a smooth (polished) plastic surface and were poured with epoxy resin. A plastic ensuring its minimum adhesion to epoxy resin was chosen. This allowed us to easily separate a sample with the particles under study after solidification of epoxy resin. Before pouring, epoxy resin was degassed in vacuum in order to decrease the amount of bubbles in it. The sample was polished with the ASM 2/1, 1/0, and 0,5/0 diamond pastes and a suspension of ultradispersed diamonds on Montasupal polishing machines on a substrate of fine cloth and felt. Nonmagnetic grains (diamonds, moissanite, corundum, etc.), after their extraction from a sedimentary rock with a heavy liquid, were mounted on plastic with the help of a needle and were subjected to ultrafine polishing.

Thermomagnetic analysis of samples from the **J** layer was performed with a magnetic balance designed by Burov, Yasonov, and Vinogradov. Pieces of about 10 $mm^3$ in volume were used for the thermomagnetic analysis, and magnetic minerals for the microprobe analysis were extracted from 100–200 $mm^3$ of the substance. The thermomagnetic analysis was first applied to a series of samples from laterally different parts of the **J** layer. Then one of the **J** layer samples was divided into six small sublayers, and magnetic minerals for electron probe examination were extracted from each sublayer by a powerful permanent magnet. The extracted particles varied in size from fractions of micron to tens of microns.

## RESULTS OF INVESTIGATIONS

A great diversity of metallic particles and microspherules of cosmic origin have been found in the Gams section in the transitional clay layer between the Cretaceous and Paleogene, as well as at two levels in the overlying Paleocene deposits. Particles and microspherules discovered in this section are considerably more diverse in shape, surface texture, and chemical composition than those detected previously in the Cretaceous–Paleogene transition layers in other regions of the world.

**Table 1.** Chemical composition (wt %) of the cosmic substance in the transitional clay layer at the Cretaceous–Paleogene boundary in the Gams section according to the data of microprobe analysis

| Element | 1 | 2 | 3 | 4 | 5 | 6 | 7 | 8 | 9 |
|---|---|---|---|---|---|---|---|---|---|
| Fe | 18.40 | 12.24 | 15.31 | 15.47 | 15.17 | 15.05 | 19.07 | 15.94 | 16.23 |
| Ni | 76.31 | 85.27 | 78.44 | 77.37 | 80.43 | 84.95 | 80.24 | 83.23 | 82.91 |
| Mn | 0.66 | – | 0.79 | 0.81 | 0.89 | – | 0.89 | 0.83 | 0.86 |
| S | 4.62 | 2.49 | 5.46 | 6.35 | 3.51 | – | – | – | – |
| Element | 10 | 11 | 12 | 13 | 14 | 15 | 16 | 17 | 18 |
| Fe | 15.31 | 15.47 | 14.70 | 14.18 | 14.94 | 33.74 | 15.78 | 15.38 | 93.83 |
| Ni | 78.44 | 77.37 | 78.28 | 79.32 | 78.77 | 51.56 | 83.23 | 83.60 | 3.95 |
| Mn | 0.79 | 0.81 | 0.97 | 0.70 | 0.91 | 0.80 | 0.99 | 1.02 | 2.20 |
| Cr | – | – | – | – | – | 2.80 | – | – | – |
| Mg | – | – | – | – | – | 7.92 | – | – | – |
| Mo | 5.46 | 6.35 | 6.05 | 5.80 | 5.38 | 3.18 | – | – | – |
| Element | 19 | 20 | 21 | 22 | 23 | 24 | 25 | 26 | 27 |
| Fe | 16.70 | 14.09 | 14.29 | 13.91 | 14.21 | 15.26 | 14.81 | 14.65 | 81.12 |
| Ni | 80.90 | 79.72 | 79.70 | 79.92 | 81.99 | 79.14 | 81.39 | 80.10 | 10.61 |
| Mn | 1.02 | 0.87 | 1.12 | 0.90 | 0.70 | 0.73 | 0.77 | – | 2.00 |
| Mo | 1.38 | 5.32 | 4.89 | 5.27 | 3.09 | 4.86 | 3.03 | 5.25 | – |
| Element | 28 | 29 | 30 | 31 | 32 | 33 | 34 | 35 | 36 |
| Fe | 16.67 | 14.96 | 15.39 | 97.72 | 71.79 | 78.04 | 15.54 | 76.87 | 72.98 |
| Ni | 81.16 | 79.24 | 80.06 | 2.28 | 3.75 | 17.61 | 80.36 | – | 2.19 |
| Mn | 0.81 | 0.98 | 0.77 | – | – | – | 0.65 | – | – |
| Mg | 1.37 | – | – | – | 20.42 | 2.83 | – | 20.67 | – |
| Cr | – | – | – | – | 2.04 | – | – | 1.42 | 24.84 |
| Mo | – | 4.82 | 3.77 | – | – | – | 3.45 | – | – |

| Element | 37 | 38 | 39 | 40 | 41 | 42 | 43 |
|---|---|---|---|---|---|---|---|
| Fe | 83.60 | 79.75 | 82.33 | 67.88 | 3.83 | 99.19 | 99.25 |
| Ni | 2.19 | 8.15 | 2.68 | 17.04 | 96.17 | – | – |
| Mn | – | – | 1.01 | – | – | 0.81 | 0.75 |
| Cr | 15.26 | 12.11 | 12.39 | 15.09 | – | – | – |
| Pt | – | – | 1.58 | – | – | – | – |

Note: 1–27, 28–35, and 36–43 are, respectively, the lower, middle, and upper parts of the transitional layer.

In the Gams section, the cosmic substance is presented by finely dispersed particles of various shapes among which magnetic microspherules 0.7 to 100 μm in size containing 98% of pure iron are most abundant [Grachev et al., 2006]. Large amounts of such particles in the shape of spheres or microspherules are found in the **J** layer and overlying Paleocene clays (in the **K** and **M** layers).

The following types of metallic microspherules have been discovered: microspherules consisting of pure iron, magnetite, or wüstite; microspherules of iron with a chromium admixture; and microspherules of pure nickel. Particles of other shapes consisting of iron–nickel alloy (awaruite) or pure nickel have also been found. Some Fe–Ni particles contain a Mo admixture. Particles of Fe-Ni alloy and pure nickel in the Cretaceous–Paleogene transition clay layer were discovered for the first time.

New results of this study are findings of particles with a high concentration of nickel and a significant amount of molybdenum, microspherules with a Cr admixture, and spiral-shaped iron. The fact that particles differing in shape and composition are confined to different parts of the transitional clay layer is also noteworthy. In addition to metallic microspherules and particles, the Gams transitional layer of clay contains Ni-

**Table 2.** Chemical composition (at %) of Ni spherules in the uppermost part of the transitional layer $\mathbf{J_6}$ according to the microprobe data

| Element | Spherule 1 | Spherule 2 | Spherule 3 |
|---|---|---|---|
| O | 6.76 | 8.66 | 9.31 |
| Na | 0.00 | – | – |
| Mg | 0.25 | – | 0.16 |
| Al | 0.61 | – | 1.04 |
| Si | 1.23 | 1.19 | 0.95 |
| P | 0.11 | – | – |
| S | 0.00 | – | 0.02 |
| Cl | 0.11 | 0.55 | 0.04 |
| K | 0.02 | – | 0.02 |
| Ca | 0.13 | 0.46 | 0.09 |
| Ti | 0.11 | 0.43 | 0.07 |
| Cr | 0.01 | – | 0.00 |
| Mn | 0.00 | – | 0.03 |
| Fe | 0.23 | – | 0.35 |
| Co | 0.02 | – | 0.07 |
| Ni | 90.41 | 88.71 | 87.85 |

spinel, microdiamonds with microspherules of pure Ni, and ragged plates of Au and Cu that are not detected in the under- and overlying deposits.

Below, we briefly characterize shapes, sizes, surface textures, and chemical compositions of all metallic particles and microspherules discovered in the transitional layer. Information on the chemical compositions of the particles is presented in Tables 1 and 2, and the compositions of spherules found in deposits of other ages are given in Table 3.

**Fe microspherules** (Fig. 3). Metallic microspherules are found in the Gams section at three stratigraphic levels. One level of findings of Fe microspherules and particles is associated with the transitional clay layer, where Fe particles of various shapes are concentrated. The second level is confined to the overlying fine-grained sandstones of the **K** layer, and the third level, to siltstones of the **M** layer (*Subbotina fringa* zone) (Fig. 3, *3*).

According to the surface morphology (texture), we distinguish spheres with a smooth surface (Fig. 3, *4–6*), a net-hummocky surface texture (Fig. 3, *1*), and a surface covered by a net of small polygonal joints (Fig. 3, *11*) or by a system of parallel joints branching from a major joint (Fig. 3, *2*).

**Table 3.** Chemical composition (wt %) of cosmic dust in various regions of the world

| Element | 1 | 2 | 3 | 4 | 5 | 6 | 7 | 8 | 9 | 10 |
|---|---|---|---|---|---|---|---|---|---|---|
| Fe | 89.48 | 25 | 44 | 80 | 75 | 70.94 | 56.01 | 4.37 | 1.11 | 0.38 |
| Ni | 9.97 | 74 | 57 | 20 | 4 | 27.63 | 38.36 | 95.47 | 98.78 | 99.94 |
| Co | 0.50 | 1 | 2 | – | 0.5 | <0.46 | 0.10 | – | – | – |
| Mn | – | – | – | – | – | 1.24 | 0.75 | 0.07 | 0.03 | 0.01 |
| Cr | – | – | – | – | – | 0.19 | 0.05 | 0.11 | 0.01 | 0.02 |
| Element | 11 | 12 | 13 | 14 | 15 | 16 | 17 | 18 | 19 | 20 |
| Fe | 22 | 72 | 10 | 71 | 68 | 66 | 60 | 44.12 | 70.08 | 7.6 |
| Ni | 76 | 2.2 | 90 | 2.3 | 4.4 | 7.3 | 3.3 | 53.96 | 28.26 | 92.7 |
| Co | 1.4 | 0.2 | 1.6 | 0.4 | 0.4 | 0.4 | 0.3 | 2.04 | 1.23 | – |
| Mn | – | – | – | – | – | – | – | – | <0.01 | – |
| Cr | – | – | – | – | – | – | – | 0.02 | – | – |

Note: The columns refer to the following objects: 1, cosmic dust [Jedwab, http://www.ub.ac.be/sciences/cosmicdust.pdf]; 2–5, magnetite globules from manganese nodules of the Atlantic and Pacific oceans [Finkelman, 1970]; 3–10, Ni–Fe spherules from Pleistocene deposits, Canada [Bi et al., 1993]; 11–14, spherules from the Tunguska catastrophe area [Florensky et al., 1968]: core (11, 13) and shell (12, 14); 18, 19, spherules from Eocene limestones, Tuamotu [Kozakevich and Disnar, 1997]; 20, a spherule from deep-sea sediments [Engrand et al., 2005].

**Fig. 3.** Fe and Ni microspherules from the Cretaceous–Paleogene transition layer in the Gams section (here and below, all photographs are made with a SEM: (*1*) Fe microspherule with a coarse net-hummocky surface texture from the upper part of the transitional **J** layer; (*2*) Fe microspherule with a coarse longitudinal-parallel surface texture from the lower part of the **J** layer; (*3*) Fe microspherule with elements of crystallographic cut and a coarse cellular-net surface texture from the **M** layer; (*4*) Fe microspherule with a fine net surface texture from the upper part of the transitional **J** layer; (*5*) Fe microspherule with a fine cellular-net surface texture from the upper part of the **J** layer; (*6*) microspherule with a fine cellular-net surface texture from the **K** layer; (*7*) Fe microspherule with a fine cellular-net surface texture from the lower part of the **J** layer; (*8*, *–9*) hollow Fe microspherule filled with clayey material (**J** layer); (*10*) metallic microspherule with a concentric inner structure from the middle part of the **J** layer; (*11*) Fe microspherule with a coarse net-hummocky surface texture from the lower part of the **J** layer; (*12*) Fe microspherule with a coarse net-hummocky surface texture from the lower–middle part of the **J** layer; (*13*) Ni microspherule with surface crystallites from the upper part of the **J** layer; (*14*) aggregate of baked Ni microspherules with surface crystallites from the upper part of the transition **J** layer; (*15*) aggregate of Ni microspherules with surface microdiamonds (C) from the upper part of the **J** layer.

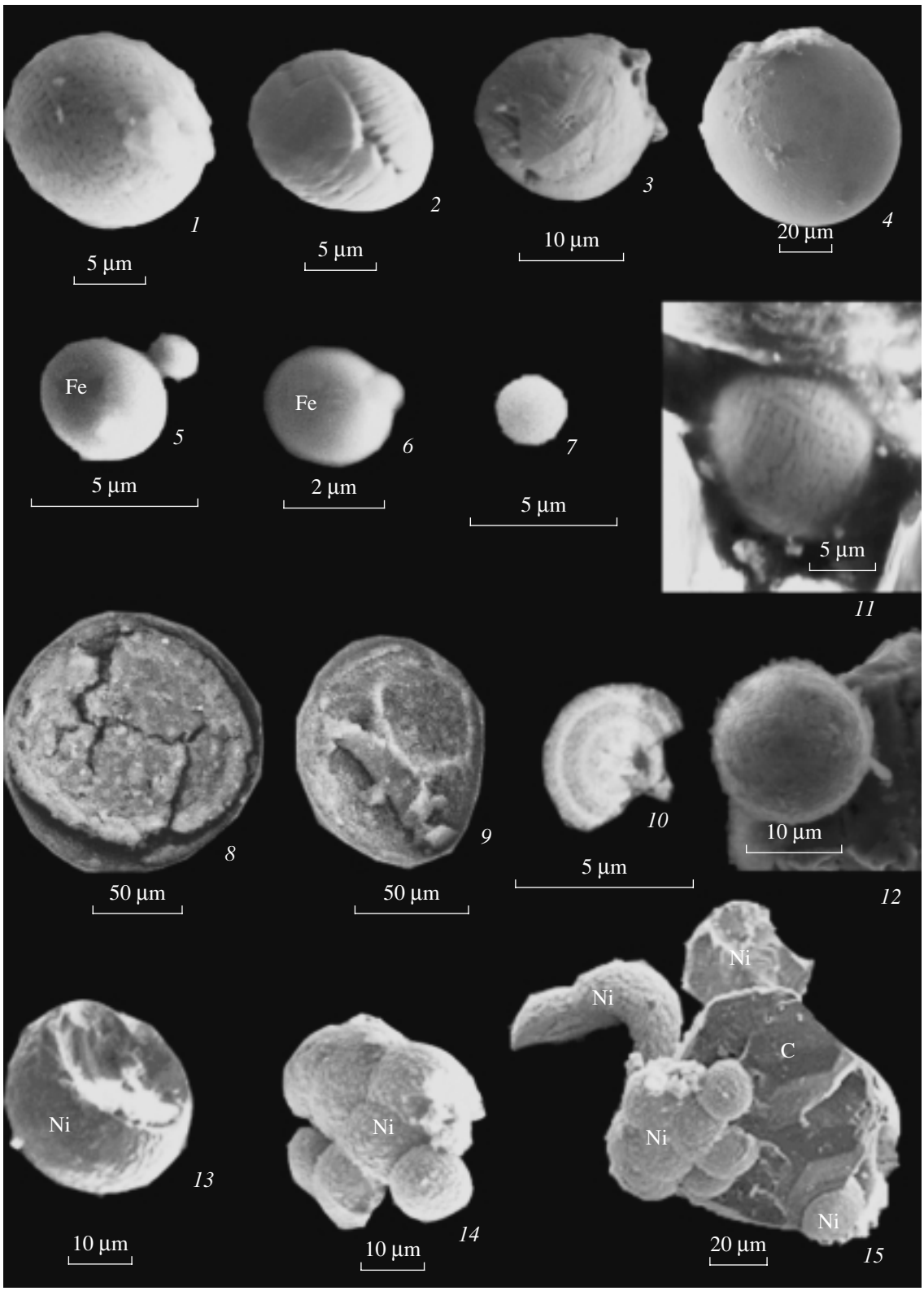
1
5 μm
2
5 μm
3
10 μm
4
20 μm
Fe
5
5 μm
Fe
6
2 μm
7
5 μm
5 μm
11
8
50 μm
9
50 μm
10
5 μm
10 μm
12
Ni
13
10 μm
Ni
14
10 μm
Ni
Ni
C
Ni
Ni
20 μm
15

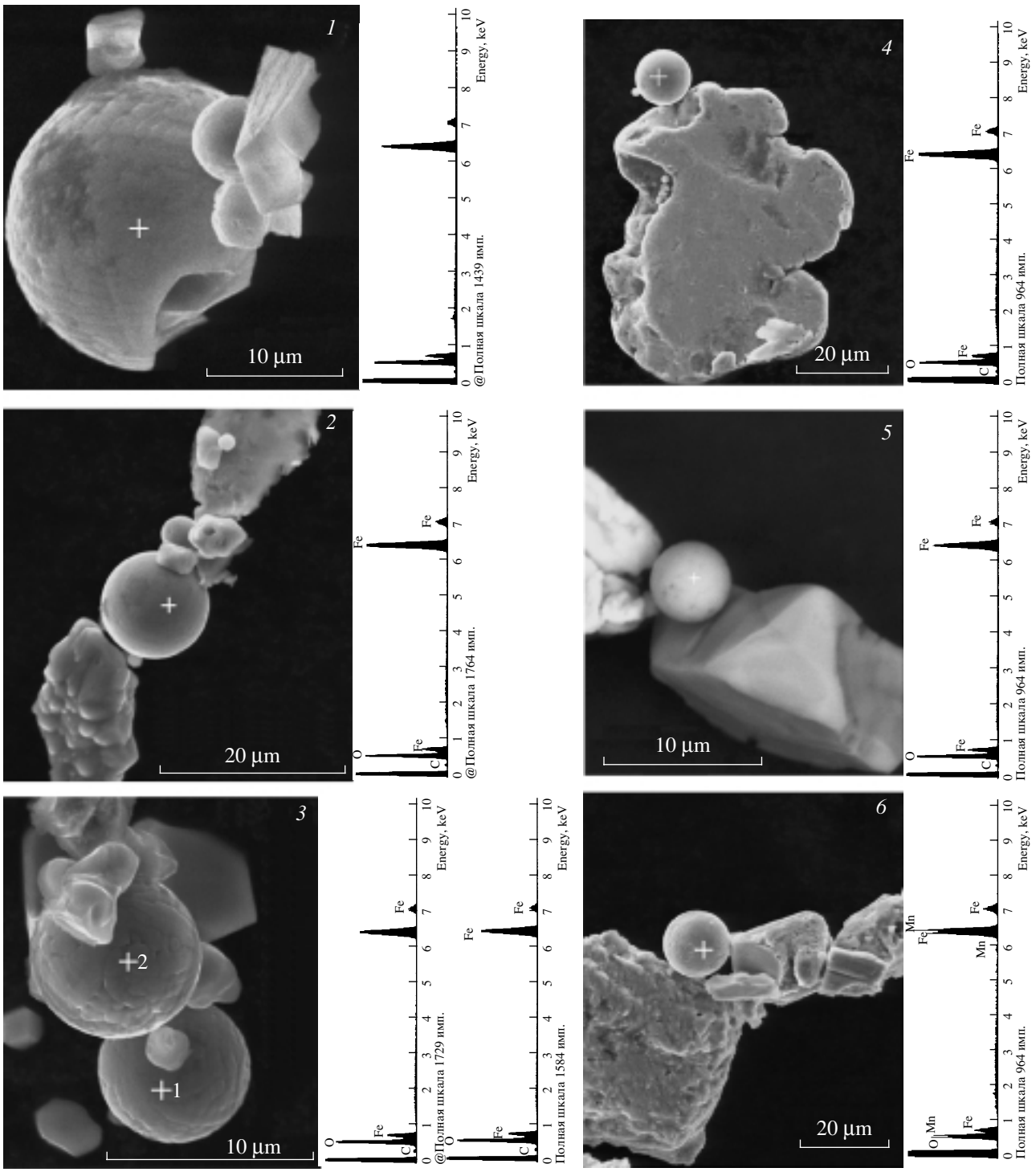


**Fig. 4.** Fe microspherules from the Cretaceous–Paleogene transition layer in the Gams section and their spectra: (*1*) coarse net-hummocky surface texture, the base of the transitional **J** layer; (*2*) fine net-cellular surface texture, the base ($\mathbf{J}_0$) of the **J** layer; (*3*) coarse net-hummocky surface texture, the base ($\mathbf{J}_0$) of the **J** layer; (*4*) fine netlike surface texture, marl of the **I** layer; (*5*) fine netlike surface texture, the lower part of the **J** layer; (*6*) fine netlike surface texture, the base (rust) of the **J** layer.

As noted above, microspherules can be hollow (Fig. 4, *1*), shell-like, or filled with a clayey mineral (Fig. 3, *8, 9*; Fig. 5, *1*), or they can have an inner concentric structure (Fig. 3, *10*). Metallic particles and Fe microspherules are met in the entire transitional layer of clay but are concentrated predominantly in its lower and middle parts.

**Micrometeorites** are represented by molten particles composed of pure Fe or Fe–Ni alloy (awaruite).

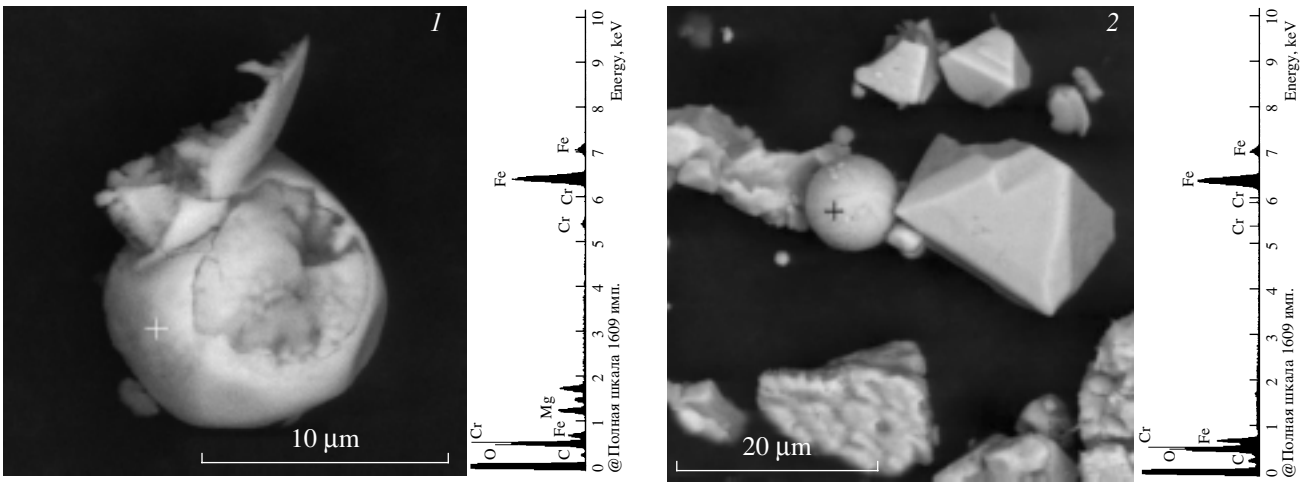


**Fig. 5.** Fe microspherules enriched in Cr from the Cretaceous–Paleogene transition layer in the Gams section and their spectra: (*1*) Fe–Cr microspherule with a coarse net-hummocky surface texture filled with clayey material, the upper part of the transitional **J** layer; (*2*) Fe–Cr microspherule with a coarse net-hummocky surface texture, the upper part of the **J** layer.

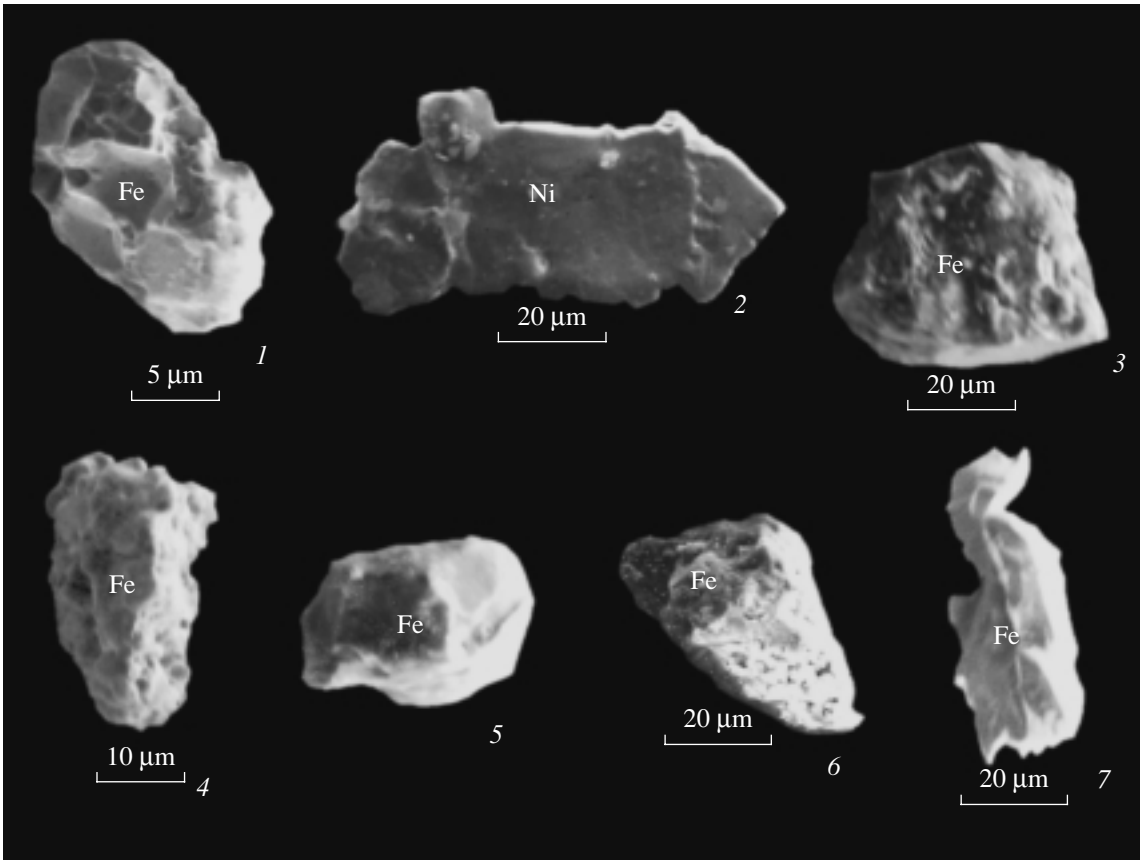


**Fig. 6.** Micrometeorites (molten metallic particles) from the Cretaceous–Paleogene transition layer in the Gams section: (*1*) Fe particle from the upper part of the transitional **J** layer; (*2*) Ni particle from the lower–middle part of the **J** layer; (*3*) Fe particle from the upper part of the **J** layer; (*4*) Fe particle from the **K** layer; (*5*) Fe particle from the upper part of the **J** layer; (*6*) Fe particle from the lower–middle part of the **J** layer; (*7*) Fe particle from the middle part of the **J** layer.

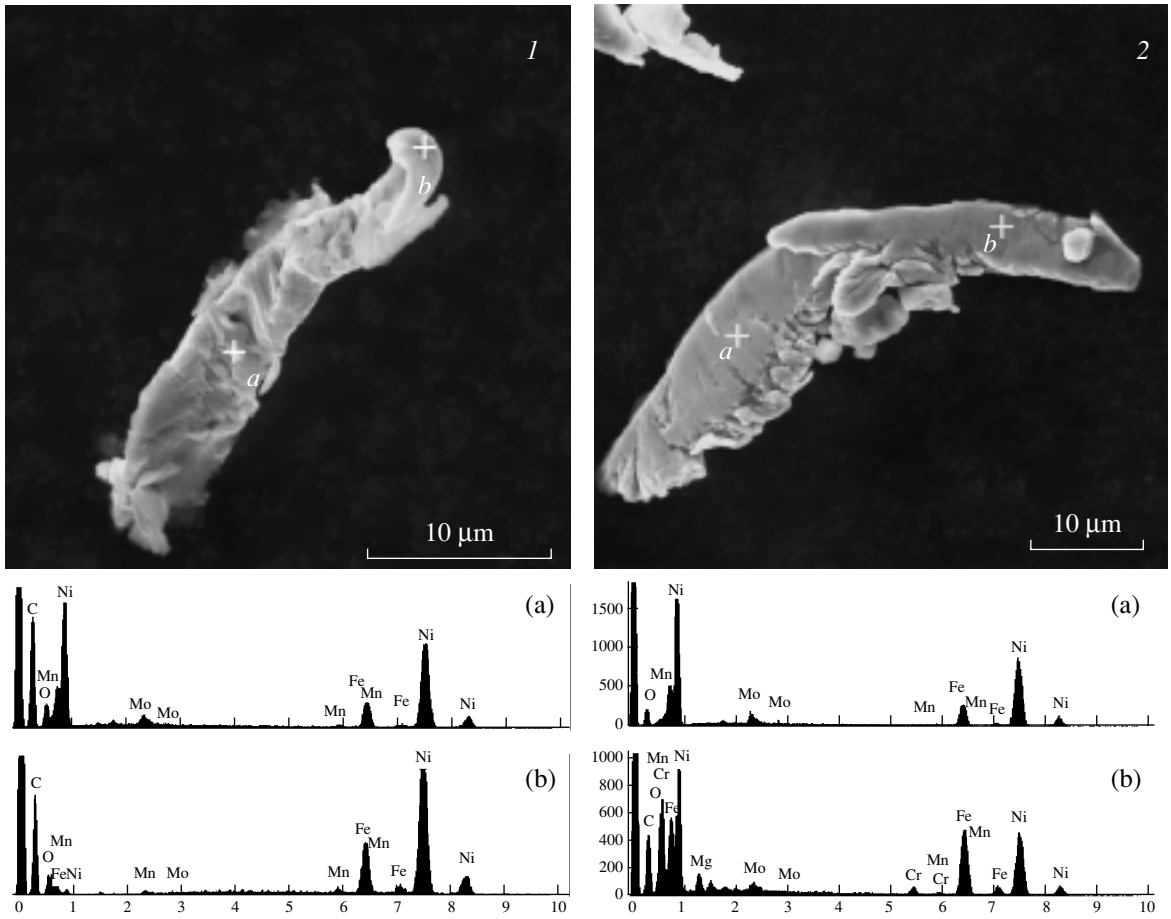


**Fig. 7.** Ni–Fe metallic particles (*1*, *2*) enriched in Mo from the base of the transitional **J** layer.

They are 5–20 μm in size (Fig. 6). Findings of numerous awaruite particles are confined to the upper part of the transitional **J** layer, whereas Fe particles are met in both the lower and upper parts of the layer.

**Fe plates with a transversely hummocky texture** (Fig. 8, *1, 2*). These slightly arched plates consist of iron alone and are 10–20 μm wide and up to 150 μm long. They are met at the base of the transitional **J** layer. Fe–Ni plates with a Mo admixture are also found in the lowermost part of the **J** layer (Fig. 7; Fig. 8, *13*).

**Ni–Fe plates with longitudinal grooves** (Fig. 8, *3*, *4*, *7*). Plates of Fe–Ni alloy have an elongated, slightly bent shape and a surface with longitudinal grooves. They are 70–150 μm long and about 20 μm wide. These plates are most widespread in the lower and middle parts of the transitional layer but are also met in its upper part.

**Fe plates with longitudinal grooves** (Fig. 8, *5*, *8*, *10*). The iron plates with longitudinal grooves coincide in shape and size with plates of Ni–Fe alloy. They are found in the lower and middle parts of the transitional layer.

**Metallic iron spirals** (Fig. 8, *10–14*). Hooked pure iron particles in the shape of a regular spiral are of particular interest. They mainly consist of pure Fe and rarely have a Fe–Ni–Mo composition (Fig. 8, *13*). Spiral-like Fe particles are met in the upper part of the transitional **J** layer and in the overlying sandstone interbed

**Fig. 8.** Metallic plates of various shapes from the Cretaceous–Paleogene transition layer in the Gams section: (*1*) Fe plate with a transverse-hummocky surface texture from the transitional **J** layer; (2a, 2b) Fe plate with a transverse-hummocky surface texture from the base of the **J** layer: (a) general view and (b) a fragment; (*3*) Ni–Fe (awaruite) particle with a concentric hummocky surface texture from the middle part of the **J** layer; (*4*) Ni–Fe (awaruite) plate with surface longitudinal grooves from the lower–middle part of the **J** layer; (*5*) Fe plate with surface longitudinal grooves from the lower–middle part of the **J** layer; (*6*) baked Fe particles with longitudinal grooves from the lower–middle part of the **J** layer; (*7*) Ni–Fe (awaruite) plate with surface longitudinal grooves from the lower–middle part of the **J** layer; (*8*) Fe plate with surface longitudinal grooves from the lower–middle part of the **J** layer; (*9*) Fe plate from the middle part of the **J** layer; (*10*) Fe plate with surface longitudinal grooves from the lower–middle part of the **J** layer; (*11*) spiral-like iron from the upper part of the **J** layer; (*12*) tubular iron from the **K** layer; (*13*) spiral-like Ni–Fe–Mo alloy from the base of the **J** layer; (*14*) tubular-twisted Fe plate from the **K** layer.

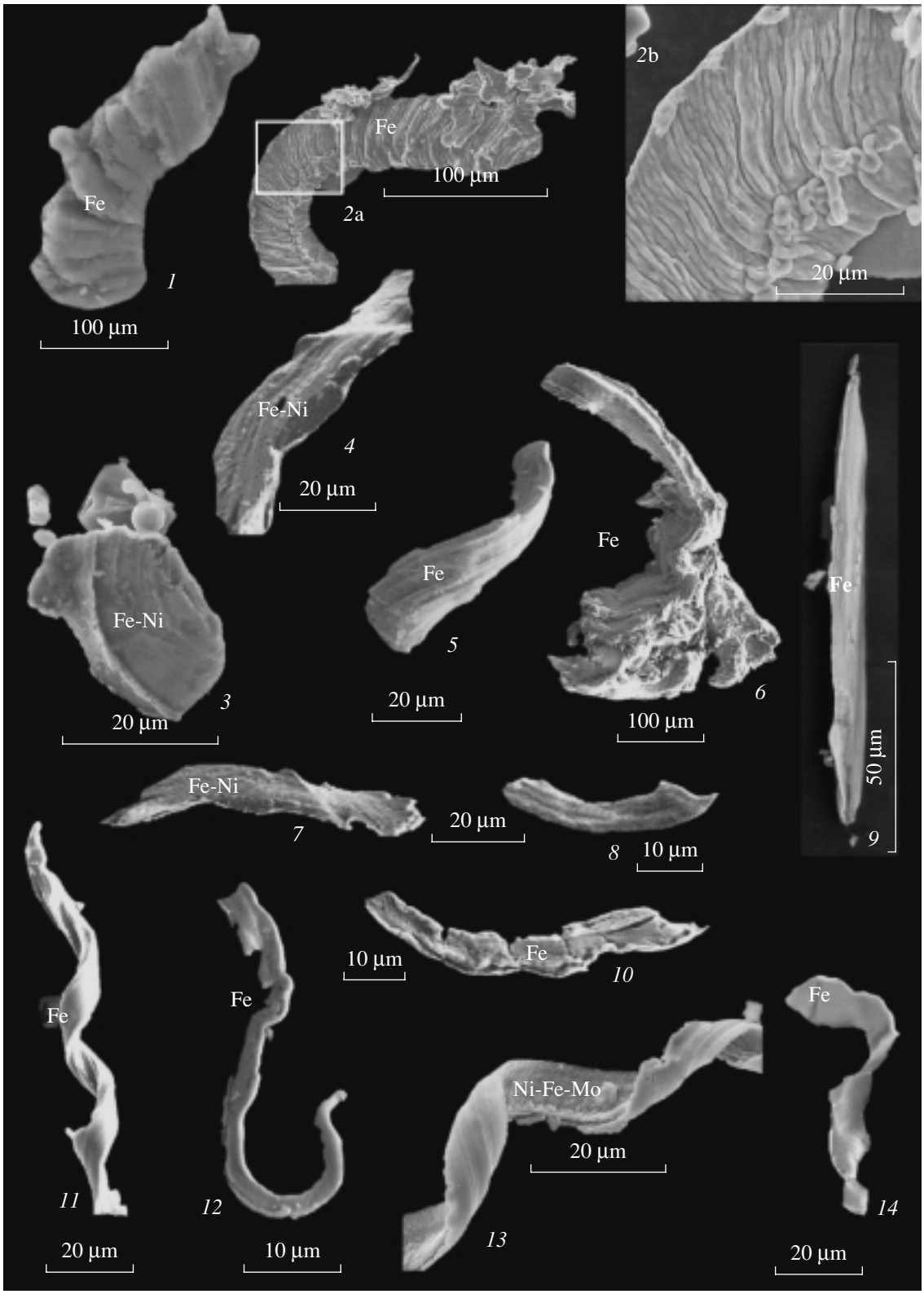
Fe
1
100 μm
Fe
100 μm
2a
2b
20 μm
Fe-Ni
4
20 μm
Fe-Ni
3
20 μm
Fe
5
20 μm
Fe
6
100 μm
Fe
50 μm
9
Fe-Ni
7
20 μm
8
10 μm
10 μm
Fe
10
Fe
Fe
11
20 μm
12
10 μm
Ni-Fe-Mo
20 μm
13
Fe
14
20 μm

(**K** layer). A spiral-like Fe–Ni–Mo particle is found at the base of the **J** layer.

**Microdiamonds and Ni microspherules** (Fig. 3, *13–15*). Several microdiamond grains baked with Ni microspherules are found in the upper part of the transitional **J** layer. The microprobe analysis of nickel spherules carried out with two instruments (equipped with wave and energy-dispersion spectrometers) showed that the Ni spherules consist of virtually pure nickel covered by a thin film of nickel oxide [Grachev et al., 2005]. The surfaces of all nickel spherules are covered with clearly observed crystallites having well-expressed twins 1–2 μm in size. Such pure nickel in the shape of spherules with a well-crystallized surface is met neither in igneous rocks nor in meteorites, where nickel invariably contains significant amounts of admixtures.

the inspection of the monolith from the section Gams 1 revealed spherules of pure Ni only in the uppermost part of the transitional **J** layer (in the very thin sedimentary layer $\mathbf{J}_6$, whose thickness does not exceed 200 μm), and data of thermomagnetic analysis indicate that metallic nickel is present in the transitional layer beginning from the $\mathbf{J}_4$ sublayer [Grachev et al., 2005; Pechersky et al., 2006]. In addition to Ni spherules, diamonds are also discovered here. A 1-cm$^2$ layer removed from a 1-cm cube contains tens of diamond grains and hundreds of nickel spherules (both ranging in size from fractions of micron to tens of microns).

The study of transitional layer samples taken directly from the outcrop revealed diamonds with fine Ni particles on the surfaces of their grains and the presence of moissanite in the upper part of the layer **J**. Previously, microdiamonds were found in the Cretaceous–Paleogene transition layer in Mexico [Hough et al., 1997].

## DISCUSSION

Iron microspherules with a net-hummocky surface detected in the Gams section are similar to microspherules of baked finely dispersed magnetite found in Pleistocene–Holocene deposits of the Morasko meteorite crater (Poland) [Stankowski et al., 2006] and microspherules with a textured surface described in [Miono et al., 1993] and are identical to microspherules of the Upper Cambrian [Korchagin et al., 2007]. According to the current ideas, a textured surface is inherent only in iron microspherules and particles associated with meteorite falls [Raukas, 2000; Stankowski et al., 2006; Szoor et al., 2001]. Thus, the discovered microspherules with a textured surface should be classified as meteoritic dust.

Microspherules with a concentric inner structure found in Gams are analogous to those discovered by the *Challenger* expedition in deep-sea clays of the Pacific [Murray and Renard, 1891]. In Gams, as well as in other regions of the world, hollow microspherules are often filled with clays.

Iron particles of an irregular shape with molten edges or in the shape of spirals and bent hooks and plates are very similar to products of destruction of meteorites falling onto the Earth and can be classified as meteoritic iron [Raukas, 2000; Szoor et al., 2001]. Particles of awaruite and pure iron can be assigned to the same category.

However, iron and nickel particles are similar in surface morphology to particles of iron and other metals emitted into the atmosphere during operation of coal power plants [Giere et al., 2003]. Note also that bent Fe particles are similar in shape to various Pele's tears, i.e., lava droplets (lapilli) ejected in the liquid state during volcanic eruptions [MacDonald, 1975].

Thus, as seen from the above, the Gams transitional layer of clay has a heterogeneous structure and is clearly subdivided into two parts: iron particles and microspherules prevail in the lower and middle parts of the layer, whereas the upper part is enriched in nickel (awaruite particles and nickel microspherules). This subdivision is confirmed not only by the distributions of iron and nickel particles in clay but also by the data of chemical and thermomagnetic analyses.

Comparison of the data of thermomagnetic and microprobe analyses indicates that the distributions of nickel, iron, and their alloy within the **J** layer are very irregular; however, according to the results of thermomagnetic analysis, pure nickel is fixed only beginning from the $\mathbf{J}_4$ layer [Grachev et al., 2005; Pechersky et al., 2006]. We should also note that helical iron is met predominantly in the upper part of the **J** layer and in the overlying **K** layer, where the amount of Fe and Fe–Ni particles of isometric or platelike shapes is small.

We should emphasize that such a distinct differentiation in iron, nickel, and iridium, which is characteristic of the transitional clay layer in Gams, is observed in other regions as well. Thus, in New Jersey (the United States), an iridium anomaly is clearly defined at the base of a 6-cm transitional (spherule) layer, whereas impact minerals concentrate only in the upper 1-cm part of the layer [Olsson et al., 2002]. Sharp enrichment in Ni and shock quartz is observed in Haiti at the Cretaceous–Paleogene boundary and in the uppermost part of the spherule layer (unit 1) [Leroux et al., 1995]. It is also noteworthy that siltstones of the **M** layer (where Fe microspherules are also met in the Gams section), belonging to the middle part of the *Subbotina fringa* zone, are close in age to the layer with an anomalously high Ir concentration in zone 1Pa(1) of the lower Danian in Haiti and to spherule layer 2 (Coxquihui section) in Mexico [Stinnesbeck et al., 2002].

## CONCLUSIONS

(1) Many characteristics of the discovered Fe and Fe-Ni spherules are analogous to those of the spherules found in deep-sea clays of the Pacific Ocean by the *Challenger* expedition [Murray and Renard, 1891], in

the Tunguska catastrophe area [Florensky et al., 1968], at the fall sites of the Sikhote-Alin' meteorite [Krinov, 1971] and Nio meteorite in Japan [Miura and Uedo, 2001], in Miocene marls of the Northern Apennines [Colombetti et al., 1996], in present-day deep-sea deposits, and in many other regions of the world (see Table 3). In all cases, except for the Tunguska catastrophe area and the fall site of the Sikhote-Alin' meteorite, the formation of both spherules and particles of various morphologies consisting of pure iron (sometimes with a Cr admixture) and Ni–Fe alloy is unrelated to impact events. We derive their formation from cosmic interplanetary dust falling onto the Earth's surface. This process has continued uninterruptedly since the moment of the Earth's formation and is, in a sense, a background phenomenon.

(2) Compositions of many particles studied in the Gams section are similar to the bulk chemical composition of the meteoritic substance found at the fall site of the Sikhote-Alin' meteorite (93.29% iron, 5.94% nickel, and 0.38% cobalt) [Krinov, 1971].

The presence of Mo in some particles is not unexpected, because this element is present in many types of meteorites. The Mo concentration in various types of meteorites (iron, stony, and carbonaceous chondrites) ranges from 6 to 7 ppm [Murthy, 1963; Campbell et al, 2003]. Most important was the discovery of molybdenite in the Allende meteorite in the form of an inclusion in metallic alloy of the following composition (in wt %): 31.1 Fe, 64.5 Ni, 2.0 Co, 0.3 Cr, 0.5 V, and 0.1 P [Fuchs and Blander, 1977]. Native molybdenum and molybdenite were also found in the composition of lunar dust collected by the Luna-16, Luna-20, and Luna-24 automatic probes [Mokhov et al., 2007].

(3) Pure nickel spherules with a well-crystallized surface found for the first time are known neither in magmatic rocks nor in meteorites, where nickel invariably contains a significant amount of admixtures. Such a surface structure of nickel spherules could have formed in the case of an asteroid (meteorite) fall, which would result in release of energy sufficient not only for melting the material of the falling body but also for its evaporation. Metal vapors could have been raised by the explosion to a large height (probably to tens of kilometers), where their crystallization took place.

(4) Awaruite ($Fe_3Ni$) particles found together with spherules of metallic nickel are a product of the meteorite ablation and belong to the category of meteoric dust, while molten iron particles (micrometeorites) should be regarded as meteoritic dust (according to Krinov's terminology [Krinov, 1971]).

(5) Diamond crystals met together with nickel spherules might have formed during ablation of meteorite from the same vapor cloud in the process of its subsequent cooling. It is known that synthetic diamonds in the shape of single crystals, their intergrowths, twins, polycrystalline aggregates, skeleton crystals, needle-shaped crystals, irregular grains, etc. are obtained by the method of spontaneous crystallization from a solution of carbon in the melt of metals (Ni, Fe) above the line of the graphite–diamond phase equilibrium [Bokii et al., 1986]. Nearly all of the above typomorphic features of diamond crystals were detected in the sample under study.

These results suggest the similarity between the diamond crystallization in the cloud of nickel–carbon vapor during its cooling and the experimental process of diamond spontaneous crystallization from a solution of carbon in a nickel melt. However, a final conclusion on the origin of diamond can be drawn after its detailed isotope investigations, which require a sufficiently large amount of substance.

Thus, the study of the transitional clay layer at the Cretaceous–Paleogene boundary revealed the presence of cosmic substance in all parts of the layer (sublayers $\mathbf{J}_1$ to $\mathbf{J}_6$); however, indicators of an impact event are fixed only beginning from the $\mathbf{J}_4$ sublayer.

## ACKNOWLEDGMENTS

This work was supported by Program no. 5 "Plume–Lithosphere Interaction" of the RAS Department of Earth Sciences, and the President of the Russian Federation, the Program for Supporting Scientific Schools, project ZSh-1901.2003.5.

## REFERENCES

1. D. Bi, R. D. Morton, and K. Wang, "Cosmic Nickel–Iron Alloy Spherules from Pleistocene Sediments, Alberta, Canada," Geochim. Cosmochim. Acta **57**, 4129–4136 (1993).
2. G. B. Bokii, G. N. Bezrukov, Yu. A. Klyuev, et al., *Natural and Synthetic Diamonds* (Nauka, Moscow, 1986) [in Russian].
3. D. E. Brownlee, "Cosmic Dust: Collection and Research," Ann. Rev. Earth Planet. Sci. **13**, 147–173 (1985).
4. D. E. Brownlee, B. A. Bates, and M. M. Wheelock, "Extraterrestrial Platinum Group Nuggets in Deep-Sea Sediments," Nature **309**, 603–605 (1984).
5. A. J. Campbell, S. B. Simon, M. Humayun, and L. Grossman, "Chemical Evolution of Metal in Refractory Inclusions in CV3 Chondrites," Geochim. Cosmochim. Acta, **67** (17), 3119–3134 (2003).
6. M. G. Chapman and D. Lauretta, "Iron Spherules from the Triassic–Jurassic Boundary Zone of the Lower Moennave, Nevada: A Preliminary Report on Possible Extraterrestrial Dust Deposits," in *32nd IGC Florence 2004, Scientific Sessions: Abstracts (Part 2),* p. 1141.
7. A. Colombetti, G. Ferrari, F. Nicolodi, and F. Panini, "Some Metallic Spherules in Calcareous–Marly Sediments of the Romahoro Flysch, Sestola-Vidiciatico Tectonic Unit (Modena District, Northern Apennines, Italy)," Planet. Space Sci. **46**, 329–340 (1998).
8. M. Ebihara and T. Miura, "Chemical Characteristics of the Cretaceous–Tertiary Boundary Layer at Gubbio,

Italy, Stevns Klint, Copper, Gold, Dust, Cerium," Geochim. Cosmochim. Acta **24**, 5133–5144 (1996).

9. M. T. Einaudi and U. B. Marvin, "Black Magnetic Spherules from Pleistocene and Recent Beach Sands," Geochim. Cosmochim. Acta **31**, 1871–1872 (1967).
10. A. El Coresy, "Metallic Spherules in Bosumtwi Crater Glasses," Earth Planet. Sci. Lett. **1**, 23–24 (1966).
11. C. Engrand, K. D. McKeegan, A. Laurie, et al., "Isotopic Compositions of Oxygen, Iron, Chromium, and Nickel in Cosmic Spherules: Toward a Better Comprehension of Atmospheric Entry Heating Effects," Geochim. Cosmochim. Acta **69**, 5365–5385 (2005).
12. K. A. Farley, "Cenozoic Variations in the Flux of Interplanetary Dust Recorded by $^3$He in a Deep-Sea Sediment," Nature **376**, 153–156 (1995).
13. V. G. Fesenkov, "Advances and Significant Problems of Meteoritics," Meteoritika, No. 31, 3–17 (1972).
14. R. B. Finkelman, "Magnetic Particles Extracted from Manganese Nodules: Suggested Origin from Stony and Iron Meteorites," Science **167**, 982–984 (1970).
15. K. P. Florensky, "Problem of Cosmic Dust and the Current State of the Study of the Tunguska Meteorite," Geokhimiya, No. 3, 284–296 (1963).
16. K. P. Florensky, A. V. Ivanov, O. A. Kirova, and N. I. Zaslavskaya, "Phase Composition of Finely Dispersed Extraterrestrial Matter of the Tunguska Meteorite," Geokhimiya, No. 10, 1174–1182 (1968).
17. L. H. Fuchs and M. Blander, "Molybdenite in Calcium–Aluminium-Rich Inclusions in the Allende Meteorite," Geochim. Cosmochim. Acta **41**, 1170–1175 (1977).
18. M. J. Genge, M. M. Crady, and R. Hutchinson, "The Texture and Compositions of Fine-Grained Antarctic Micrometeorites: Implications for Comparisons with Meteorites," Geochim. Cosmochim. Acta **61**, 5149–5162 (1997).
19. R. Giere, L. E. Carleton, and G. R. Lumpkin, "Micro- and Nanochemistry of Fly Ash from a Coal-Fired Plant," Am. Mineral. **88**, 1853–1863 (2003).
20. A. F. Grachev, O. A. Korchagin, H. A. Kollmann, et al., "A New Look at the Nature of the Transitional Layer at the K/T Boundary Near Gams, Eastern Alps, Austria, and the Problem of the Mass Extinction of the Biota," Russ. J. Earth Sci. **7**, 1–45 (2005).
21. A. F. Grachev, O. A. Korchagin, and V. A. Tsel'movich, "Cosmic Matter in Clay at the Cretaceous–Paleogene Boundary (Gams, Eastern Alps)," *Physicochemical and Petrophysical Research in Earth Sciences* (IFZ RAN, Moscow, 2006) [in Russian].
22. A. F. Grachev, V. A. Tsel'movich, O.A. Korchagin, and H. A. Kollmann, "Two Spinel Populations from the Cretaceous–Paleogene (K/T) Boundary Clay Layer in the Gams Stratigraphic Sequence, Eastern Alps," Russ. J. Earth Sci. **10** (2), 1–11 (2007a).
23. A. F. Grachev, I. L. Kamenskii, O. A. Korchagin, and H. A. Kollmann, "The First Data on Helium Isotopy in a Transitional Clay Layer at the Cretaceous–Paleogene Boundary (Gams, Eastern Alps)," Fiz. Zemli, No. 9, 61–67 (2007b).
24. W. T. Holser and M. Magaritz, "Cretaceous/Tertiary and Permian/Triassic Boundary Events Compared," Geochim. Cosmochim. Acta **56**, 3297–3309 (1997).
25. R. M. Hough, I. Gilmour, C. T. Pillinger, et al., "Diamonds from the Iridium-Rich K/T Boundary Layer at Arroyo El Mimbral, Namaulipas, Mexico," Geology **25**, 1019–1022 (1997).
26. W. Hunter and D. W. Parkin, "Cosmic Dust in Recent Deep-Sea Sediments," Proc. R. Soc. Ser. A, Math. Phys. Sci. London **255** (1282), 382–397 (1960).
27. A. V. Ivanov and K. P. Florensky, "Intensity of Fallout of Finely Dispersed Cosmic Matter onto the Earth," Geokhimiya, No. 11, 1365–1372 (1970).
28. J. Jedwab, "Cosmic Dust in Manganese Nodules. Pictures from the Report on "Deep-Sea Deposits" of the H.M.S. Challenger's Expedition (http://www,ub.ac.be/sci.erices/cosinicdust.pdf).
29. D. B. Karner, J. Levine, R. Muller, et al., "Extraterrestrial Accretion from the GISP2 Ice Core," Geochim. Cosmochim. Acta **67**, 751–763 (2003).
30. G. Keller and W. Stinnesbeck, "Iridium and the K/T Boundary at El Caribe, Guatemala," Int. J. Earth Sci. **88**, 840–843 (2002).
31. G. Keller, T. Adatte, W. Stinnesbeck, et al., "Paleoecology of the Cretaceous–Tertiary Mass Extinction in Planktonic Foraminifera," Palaeogeogr. Palaeoclimatol. Palaeoecol **178**, 257–292 (2002).
32. H. A. Kollmann, "Stratigraphie und Tectonik des Gosaubeckens von Gams (Steirmark, Osterreich)," Jb. Geol. **107**, 71–159 (1963).
33. O. A. Korchagin, S. V. Dubinina, V. A. Tsel'movich, and I. I. Pospelov, "Possible Impact Event in the Late Cambrian," Global Geol. **10** (2007).
34. A. Kosakevitch and J. R. Disnar, "Nature and Origin of Chemical Zoning in the Metal Nucleus and Oxide Cortex of Cosmic Spherules from the Tuamotu Archipelago, French Polynesia," Geochim. Cosmochim. Acta **61**, 1073–1082 (1997).
35. D. Kring and W. V. Boyton, "Altered Spherules of Impact Melt and Associated Relic Glass from the K/T Boundary Sediments in Haiti," Geochim. Cosmochim. Acta **55**, 1737–1742 (1991).
36. E. L. Krinov, "New Studies of the Fallout and Findings of the Sikhote-Alin' Meteorite Shower," in *Problems in Cosmochemistry and Meteoritics* (Naukova Dumka, Kiev, 1971), pp. 117–128 [in Russian].
37. Kurat, C. Koeberl, T. Presper, et al., "Petrology and Geochemistry of Antarctic Micrometeorites," Geochim. Cosmochim. Acta **58**, 3879–3904 (1994).
38. F. T. Kyte and J. T. Wasson, "Accretion Rate of Extraterrestrial Matter: Iridium Deposited 33 to 7 Million Years Ago," Science **232**, 1225–1229 (1986).
39. R. Lahodynsky, "Lithostratigraphy and Sedimentology across the Cretaceous/Tertiary Boundary in the Flyschgosau (Eastern Alps, Austria)," Riv. Espanola de Paleontologia. N Extraordinario, 73–82 (1988).
40. H. Leroux, R. Rocchia, L. Froget, et al., "The K/T Boundary at Beloc (Haiti): Compared Stratigraphic Distributions of the Boundary Markers," Earth Planet. Sci. Lett. **132**, 255–268 (1995).
41. B. Yu. Levin and A. N. Simonenko, "The Earth among Dust and Stones," Priroda, No. 4, 7–14 (1973).

42. G. A. MacDonald, *Volcanoes* ((Prentice-Hall, Englewood Cliffs, N.J., 1972; Mir, Moscow, 1975) [in Russian].
43. F. Marcantonio, N. Kumar, M. Stute, et al., "A Comparative Study of Accumulation Rates Derived by He and Th Isotope Analysis of Marine Sediments," Earth Planet. Sci. Lett. **133**, 549–555 (1995).
44. F. Martinez-Ruiz, M. O. Huertas, I. Palomo, and P. Acquafredda, "Quench Textures in Altered Spherules from the Cretaceous–Tertiary Boundary Layer at Agost and Caravaca, SE Spain," Sedimentary Geol. **113** (1997).
45. U. B. Marvin and M. T. Einaudi, "Black Magnetic Spherules from Pleistocene Beach Sands," Geochim. Cosmochim. Acta **3**, 1871–1884 (1967).
46. M. Maurette, C. Jehanno, E. Robin, and C. Hammer, "Characteristics and Mass Distribution of Extraterrestrial Dust from the Greenland Ice Cap," Nature **328**, 699–702 (1986).
47. S. Messenger, F. J. Stadermann, C. Floss, et al., "Isotopic Signatures of Presolar Materials in Interplanetary Dust," Space Sci. Rev. **106**, 155–172 (2003).
48. S. Miono, Y. Nakayama, M. Shoji, et al., "Origin of Microspherules in Paleozoic–Mesozoic Bedded Chert Estimated by PIXE Analysis," Nuclear Instruments and Methods in Physics Research, **B75**, 435–439 (1993).
49. Y. Miura and Y. Uedo, "Iron Spherules and Melted Fragments Found at Rice-Field of Nio Meteorite Shower Site in Yamaguachi, Japan," Lunar Planet. Sci. **XXXII** (2001).
50. A. V. Mokhov, P. M. Kartashov, and O. A. Bogatikov, *Moon under a Microscope* (Nauka, Moscow, 2007) [in Russian].
51. S. Murray and A. F. Renard, *Report on Deep-Sea Deposits Based on the Specimens Collected during the Voyage of H.M.S. Challenger in the Years 1872 to 1876* (Neil, Edinburgh, 1891), Vol. 3.
52. V. R. Murthy, "Elemental and Isotopic Abundances of Molybdenum in Some Meteorites," Geochim. Cosmochim. Acta **27**, 1171–1178 (1963).
53. R. K. Olsson, K. G. Miller, J. V. Browning, et al., "Sequence Stratigraphy and Sea-Level Change across the Cretaceous–Tertiary Boundary on the New Jersey Passive Margin," Geol. Soc. Am. Sp. Pap. **356**, 97–108 (2002).
54. D. W. Parkin, R. A. L. Sullivan, and J. N. Andrews, "Further Studies on Cosmic Spherules from Deep-Sea Sediments," Phil. Trans. R. Soc. London. Ser. A. Math. Phys. Sci. **297**, 495–518 (1980).
55. J. N. Pattan, N. J. G. Pearce, V. K. Banakar, and G. Parthibian, "Origin of Ash in the Central Indian Basin and Its Implication for Volume Estimate of the 74000 Year BP Youngest Toba Eruption," Current Sci. **83**, 889–892 (2002).
56. D. M. Pechersky, A. F. Grachev, D. K. Nourgaliev, et al., Magnetolithologic and Magnetomineralogic Characteristics of Deposits at the Mesozoic/Cenozoic Boundary: Gams Section (Austria)," Russian J. Earth Sci. **8** (3) (2006).
57. A. Raukas, "Investigation of Impact Spherules—A New Promising Method for the Correlation of Quaternary Deposits," Quaternary Int. **68–71**, 214–252 (2000).
58. S. N. Rychagov, S. F. Glavatskikh, and E. I. Sandimirova, "Ore and Silicate Magnetic Spherules as Indicators of the Structure and Fluid Regime of the Contemporary Baranskii Hydrothermal System (Iturup Island)," Dokl. Akad. Nauk **356**, 671–681 (1997).
59. B. Schimitz, M. Lindsrom, F. Asaro, and M. Tassari, "Geochemistry of Meteorite-Rich Marine Limestone Strata and Fossil Meteorites from the Lower Ordovician at Kinnekulle, Sweden," Earth Planet. Sci. Lett. **145**, 31–48 (1996).
60. A. N. Simonenko and B. Yu. Levin, "Cosmic Matter Influx onto the Earth," Meteoritika, No. 31, 45–56 (1972).
61. J. Smit and A. J. T. Romein, "A Sequence of Events across the Cretaceous–Tertiary Boundary," Earth Planet. Sci. Lett. **74**, 155–170 (1985).
62. E. V. Sobotovich, *Cosmic Matter in the Earth's Crust* (Atomizdat, Moscow, 1976) [in Russian].
63. E. V. Sobotovich, G. N. Bondarenko, and T. I. Koromyslechenko, *Cosmic Matter in Oceanic Sediments and Glacial Covers* (Naukova Dumka, Kiev, 1978) [in Russian].
64. F. J. Stadermann, Ch. Floss, and B. Wopenka, "Circumstellar Aluminum Oxide and Silicon Carbide in Interplanetary Dust Particles," Geochim. Cosmochim. Acta **70**, 6168–6179 (2006).
65. W. T. J. Stankowski, A. Katrusiak, and A. Budzianowski, "Crystallographic Variety of Magnetic Spherules from Pleistocene and Holocene Sediments in the Northern Foreland of Morasko-Meteorite Reserve," Planet. Space Sci. **54**, 60–70 (2006).
66. W. Stinnesbeck, G. Keller, P. Schulte, et al., "The Cretaceous–Tertiary (K/T) Boundary Transition at Coxquinhui, State Veracruz, Mexico: Evidence for an Early Danian Impact Event?," J. South Am. Earth Sci. **15**, 497–509 (2002).
67. Gy. Szoor, Z. Elekes, P. Rozsa, et al., "Magnetic Spherules: Cosmic Dust Or Markers of a Meteoritic Impact?," Nuclear Instrum. Methods in Phys. Res. Ser. B **181**, 557–562 (2001).
68. G. Winckler and H. Fisher, "30 000 Years of Cosmic Dust in Antarctic Ice," Science **313**, 491 (2006).
69. T. Yada, T. Nakamura, N. Takaoka, et al., "The Global Accretion Rate of Extraterrestrial Materials in the Last Glacial Period Estimated from the Abundance of Micrometeorites in Antarctic Glacier Ice," Earth Planets Space **56**, 67–79 (2004).

SPELL: 1. clayey, 2. marly